IfG Institut für Gebirgsmechanik GmbH
Untersuchung - Prüfung - Beratung - Begutachtung

Rock-Mechanical Laboratory Investigations

on Rock Salt from the AKZO Nobel well ISH-01

Contractor: DEEP. Underground GmbH, Bad Zwischenahn

Purchase Order No. : 22990 dated 08/05/2011

Project No. : 5304-880591

Order No. (IfG): IfG 43/2011

Authors: 5.1.2.e

Leipzig, 18/07/2012

5.1.2.e

Table of contents

1. Rock-mechanical investigation program

Since 1933, with the opening of the Twente canal, AkzoNobel has been mining salt in concession areas near the cities of Hengelo and Enschede. Using solution mining, Triassic Röt salt is being mined from caverns at depths ranging from 300 to 500 meters. The present mining locations all are situated within the Twenthe-Rijn and Twenthe-Rijn Uitbreiding concession areas. As an extension of salt exploitation in these locations is not possible, AkzoNobel is investigating salt mining possibilities in new areas in the eastern part of the Netherlands and at other, deeper geological layers, like the Permian Zechstein salt.

Since 2006, AkzoNobel has been investigating the geological situation in the area around Hengelo and Enschede to get insight into its future salt mining prospects. This investigation was conducted in several steps: firstly a regional geological study by the American company Respec, and secondly a more thorough modelling study by MWH were conducted, both using borehole and seismic data. On the basis of the improved model and the previously gathered information on spatial requirements, it was then possible to make a first selection of six so-called ‘areas of interest’ that seemed to offer good opportunities for future salt mining. The evaluation of these areas of interest indicated that the best prospects for future salt mining are located in the Haaksbergen area. Within this area salt mining from relatively shallow Zechstein salt resources was classified to be technically feasible and economically profitable.

As part of the permitting procedure for mining, a detailed investigation program was launched by AkzoNobel including the drilling of the exploration well ISH-01. Cores retrieved from this well were available for rock-mechanical lab-tests in order to determine the site-specific mechanical characteristics of the salt.

The present report describes the methods, the technique and the results of the performed rock-mechanical laboratory tests using site-specific core material from well ISH-01. The main targets of the rock-mechanical tests are:

- to verify the strength resulting from triaxial compression tests applying different pressure conditions,
- to determine the permissible utilization of the short-term strength from relaxations tests with respect to a limited deformation of the surrounding rock salt mass and typical deformation rates of some $^{o}/_{oo}$ per year,

- to measure elastic parameters by applying rapid cycles of mechanical loading and unloading, and
- to describe the creep behavior of the rock salt under triaxial stress conditions providing primary creep as well as secondary creep parameters including time dependent healing.

To determine the different rock-mechanical behavior/parameters, the rock-mechanical test program is performed on cores from the Z1 (Werra) Zechstein Formation selected at different depths in well ISH-01. The cores are retrieved from diverse coring jobs. The core selection is done after consultation with the client.

The detailed test program comprises the following tests:

1. Triaxial compression tests (TC) with constant deformation rate (9 %/h):
   14 tests on larger specimens (…diameter?) applying confining pressures in the range of 0.2 – 25 MPa and 26 tests on smaller specimens (…diameter?) applying comparable pressure conditions are carried out.

2. Triaxial compression tests with relaxation phases (TCR) at 5 and 10 % axial deformation:
3. 4 tests in the range of confinement pressures comparable to the conditions of the TC-tests are conducted

4. Long-term tests in order to determine the time dependent creep behavior under triaxial conditions as well as in compression and extension. 16 tests under confining pressures between 5 – 20 MPa with applied axial loads in a range between 10 – 25 MPa are performed.

5. 4 shear tests are carried out in order to determine the cohesion and the friction angle of bedding planes between rock salt/anhydrite.

A complete overview of the specimens tested in the laboratory is given in tab 1.1.

Table 1.1: Overview of tested specimens

specimen	depth	hight	diameter	mass	density	p-wave velocity	s-wave velocity
	[m]	[mm]	[mm]	[g]	[t/m3]	[km/s]	[km/s]
461/06/37/TC1	683	180,25	90,15	2493,70	2,168	3,173	##
461/8/52/TC2	697	180,34	90,19	2498,60	2,169	2,240	##
461/11/70/TC3	713	180,44	90,22	2495,30	2,163	##	##
461/13/85/TC4	725	180,21	90,25	2513,00	2,180	##	##
461/18/118/TC5	754	180,18	90,12	2484,70	2,162	2,399	##
461/24/165/TC6	794	180,23	90,21	2478,20	2,152	##	##
461/27/185/TC7	811	180,24	90,25	2495,50	2,164	4,447	2,155
461/30/206/TC8	831	180,03	90,26	2481,70	2,154	##	##
461/33/226/9	847	180,10	90,15	2478,30	2,156	4,057	##
461/39/266/10	882	180,37	90,05	2484,90	2,163	4,253	2,404
461/41/280/TC11	894	180,27	90,17	2476,00	2,151	2,984	1,730
461/43/296/TC12	907	179,93	90,31	2512,40	2,180	4,185	2,295
461/46/317/TC13	925	180,20	90,18	2485,70	2,160	##	##
461/50/346/TC14	951	180,07	90,16	2498,80	2,174	##	##
461/8/52/K3	697	80,28	40,15	218,27	2,148	1,467	##
461/10/66/K5	709	80,34	40,25	220,00	2,153	2,054	##
461/11/70/K7	713	80,17	40,21	218,45	2,146	##	##
461/16/109/K9	746	80,33	40,12	219,67	2,163	##	##
461/16/109/K11	746	80,33	40,11	218,22	2,150	##	##
461/18/118/K13	754	80,34	40,20	218,17	2,140	##	##
461/21/144/K15	776	80,39	40,41	222,80	2,161	4,165	1,670
461/21/144/K16	776	80,02	40,21	218,82	2,154	4,356	1,813
461/21/144/K17	776	80,52	40,20	221,39	2,166	4,638	1,974
461/26/178/K21	805	80,18	40,14	219,16	2,161	4,058	2,407
461/27/185/K23	811	80,34	40,36	221,12	2,152	4,849	2,252
461/27/185/K24	811	80,15	40,31	220,36	2,155	4,805	1,823
461/29/197/K25	822	80,16	40,31	219,45	2,145	4,724	2,082
461/32/217/K29	839	80,01	40,25	218,73	2,149	4,554	2,223
461/33/226/K31	847	80,26	40,27	220,23	2,154	4,583	2,183
461/33/226/K32	847	80,19	40,20	219,03	2,153	4,646	2,306
461/39/266/K35	882	80,20	40,02	218,30	2,164	4,045	2,341
461/39/266/K36	882	80,31	40,22	222,87	2,184	4,479	2,437
461/41/280/K38	894	80,25	40,13	219,27	2,161	1,706	##
461/43/296/K39	907	80,27	40,31	221,21	2,159	4,442	2,039
461/46/317/K42	925	80,18	40,31	220,19	2,152	4,174	2,000
461/30/206/K44	831	80,30	40,33	219,38	2,139	4,636	2,429
461/33/226/K45	847	80,20	40,31	219,32	2,143	4,371	##
461/43/296/K46	907	80,17	40,33	220,19	2,150	4,519	2,144
461/8/52/K2	697	80,36	40,17	223,47	2,195	4,324	0,783
461/8/52/K4	697	80,17	40,18	222,38	2,188	4,320	##
461/10/66/K6	709	80,01	40,18	218,56	2,154	4,159	##
461/11/70/K8	713	80,16	40,14	218,43	2,154	5,186	##
461/16/109/K10	746	80,03	40,19	219,38	2,161	4,156	##
461/16/109/K12	746	80,00	40,19	219,23	2,161	4,635	##
461/18/118/K14	754	80,08	40,19	219,19	2,158	4,068	1,041
461/21/144/K18	776	80,14	40,28	222,20	2,176	4,220	2,710
461/23/158/K20	789	80,21	40,32	221,26	2,160	4,320	2,659
461/26/178/K22	805	79,98	40,25	220,18	2,164	4,440	2,529
461/29/197/K26	822	80,02	40,27	219,55	2,155	4,173	2,718
461/29/197/K28	822	79,95	40,30	218,58	2,143	3,996	2,660
461/32/217/K30	839	80,17	40,27	219,62	2,151	4,721	2,792
461/38/262/K34	878	79,96	40,18	220,65	2,177	4,517	2,740
461/41/280/K37	894	80,07	40,16	219,06	2,160	4,240	2,406
461/43/296/K40	907	80,01	40,25	219,59	2,157	4,268	2,518
461/46/317K41	925	80,21	40,23	218,59	2,144	##	##
461/29/197/K27	822	79,99	40,30	219,44	2,151	4,52	2,40
461/23/158/K19	789	80,49	40,26	220,34	2,150	##	##

2. Laboratory Equipment at IfG

For rock-mechanical investigations the following facilities and equipment are available in the laboratory of IfG:

a) Climate-controlled rooms to store the core material and the specimens at conditions which correspond to those in-situ.
b) Laboratory for mineral-petrographical examinations, density and moisture determination, ultra-sonic measurements and photographical documentation.
c) Workshop for high-precision specimen preparation according to the test requirements based on international standards.
d) Geomechanical investigation and test laboratory containing a:
   - *Computer network with various program systems for data recording and data evaluation.*
   - *Servo-controlled hydraulic testing machine, system RBA 2500 (maximum axial load: 2.5 MN) with 2 triaxial cells (test specimens up to 110 mm diameter and 220 mm length) for confining pressures of up to 100 MPa as well as test temperatures in the range 295 – 400 K.*

Fig: 2.1. The RBA 2500 test system (right) and the SHM 250 test system (left)

   - *Servo-controlled hydraulic testing machine, system SMH 250 (maximum axial load: 250 kN) with several triaxial cells (test specimens up to 40 mm diameter and 100 mm length) for confining pressures of up to 50 MPa as well as test temperatures in the range 295 - 400 K .*

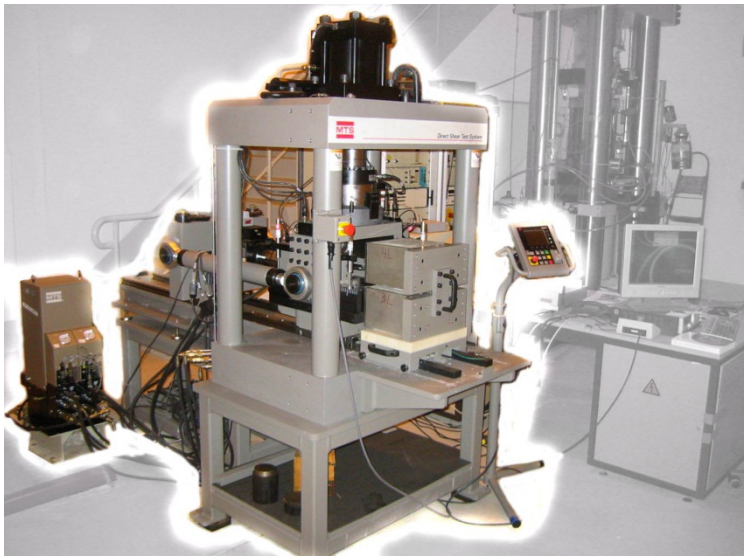

Fig: 2.2. The MTS – shear test system model 816

- High-response servo-hydraulic systems with digital control *for MTS shear test system.* The loading frame consists of a two-axle experimental setup with vertical and horizontal stress initiation. A servo-hydraulic control unit for two channels (vertical and horizontal), can be managed force or displacement controlled. The test arrangement is shown in Fig. 2.2. The horizontal force is generated by a laterally positioned horizontal cylinder (- 250 kN compression; - 160 kN tension), while in vertical direction a 500 kN hydraulic cylinder is operating.

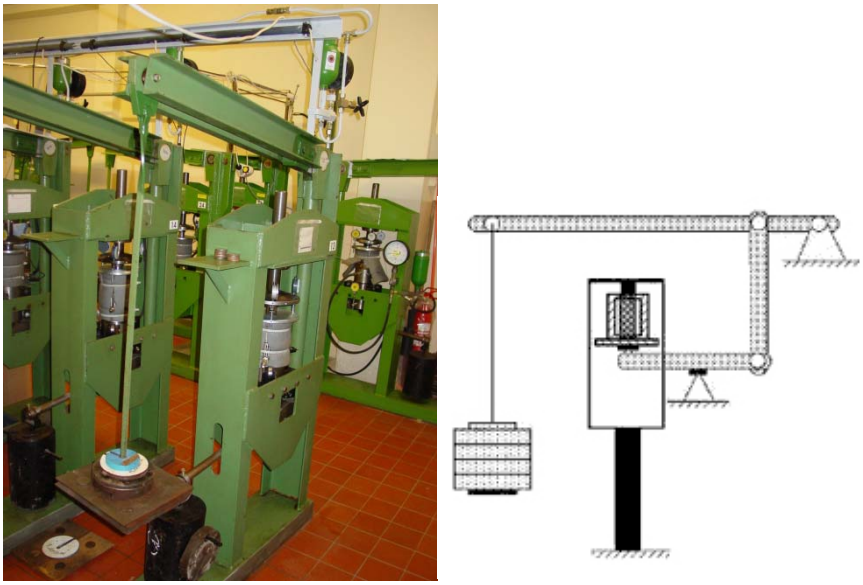

Fig: 2.3. The creep test rig with a sketch of its principal work

- *36 testing rims (Fig. 2.3) for long-term creep tests in climate-controlled laboratories, with triaxial cells for testing in compressional and extensional loading, which can be heated up to 120 °C. The test conditions can be varied applying confining pressures up to 30 MPa, while axial loads are possible up to 200 kN.*

3. Determination of the physical rock parameters

After preparing the cylindrically shaped specimens their densities are determined by measuring the geometrical dimensions and their mass. Table 1.1 summarizes these parameters and some additional information, e.g. sample depths and the test conditions.

Concerning the quality of the measurement parameters it has to be mentioned that the accuracy of the length measurement is higher than 0.02 mm and for mass determination less or equal than 0.02 g.

Ultrasonic investigations are carried out to check integrity, homogeneity and isotropy of the specimens. The ultrasonic pulse measurement system USD10NF, which is used for sound transmission of the rock specimens, consists of two transducer sets (0.5 MHz) for p-waves and s-waves respectively, and the Krautkramer-Receiver-System for generating and evaluating the ultrasonic signals. The specimen is placed between two piezoelectric transducers, of which one acts as the driver and the other as the receiver. The transition time of the mechanical pulse to pass through the specimen is used to calculate the elastic wave velocity.

The elastic constants are obtained from density (ρ) and the ultrasonic velocities (v_p, v_s) using the equations 1 and 2 which are based on the theory of elasticity for homogeneous, isotropic solids:

$$E_{dyn} = \frac{\rho \cdot v_s^2 \cdot \left(3 \cdot v_s^2 - 4 \cdot v_s^2\right)}{v_s^2 - v_s^2} \quad (1)$$

$$\nu_{dyn} = \frac{v_s^2 - 2 \cdot v_s^2}{2 \cdot \left(v_s^2 - v_s^2\right)} \quad (2)$$

Dynamic elastic parameters, which are calculated for the rock salt from ultrasonic wave velocities at room temperature, are describing the degree of homogeneity of the core

material with regard to its density and bulking. Based on the test results these characteristics for the ISH-01 core material are:

$$E_{dyn} = 24 \ldots 33 \text{ GPa}$$

$$K_{dyn} = 22 \ldots 29 \text{ GPa}$$

$$\nu_{dyn} = 0.23 \ldots 0.30$$

4. Rock-mechanical laboratory investigations

4.1. Triaxial compression and relaxation tests

4.1.1. Test procedure

Triaxial compression tests (TC) are carried out with the servo-hydraulic controlled test machines RBA 2500 and SHM 250.

Generally, triaxial testing is subdivided into several test stages. The first one represents a hydrostatic loading with axial and confining stress at the same level ($\sigma_1 = \sigma_3$) until the estimated former overburden pressure is achieved. This is followed by an unloading step with constant deformation rate down to confining pressure that is intended to be investigated at a subsequent test. The hydrostatic loading is increased by a pressure growth rate of 1 bar/s.

The determination of the elastic parameters as Young's modulus E, compression modulus K and Poisson's ratio ν is based on Hook's law according to equation 3.

$$\Delta\varepsilon_1 \cdot E = \Delta\sigma_1 + 2\nu \cdot \Delta\sigma_3 \qquad (3)$$

The terms $\Delta\varepsilon_1$ and $\Delta\sigma_1$ are variations of the axial deformation and the axial load, while $\Delta\sigma_3 = \Delta p$ is a variation of the confining pressure. The elastic parameters were measured for an appropriate amount of stress variation during loading and unloading cycles.
Appling equation (3) the Young's modulus E results from $\Delta\sigma_3 = 0$

$$E = \frac{\Delta\sigma_1}{\Delta\varepsilon_1} \qquad (4)$$

The compression modulus K results from equations (4) and (5) while setting $\Delta\sigma_1 = \Delta\sigma_3 = \Delta p$

$$3K = \frac{\Delta\varepsilon_1}{\Delta p} \qquad (5)$$

and using the following equation (6).

$$K = \frac{E}{3 \cdot (1 - 2\nu)} \qquad (6)$$

Following the test procedure a variety of confining pressures between 0.2 and 20 MPa (see fig. 4.1.1 and 4.1.2) are applied for each individual test. Axial strains are set to ε_1 = 0 % after the confining pressure is applied. The specimens are loaded using a constant deformation rate of $\dot{\varepsilon}_1 = 2.5 \cdot 10^{-5}\,s^{-1}$. Testing temperatures are kept at room temperature for all strength tests.

Some tests include relaxation phases, e.g. the deformation is stopped at 5% and 10% and the stress decay is observed. These relaxation tests are a unique method to prove the inherent long-term deformation behavior of rock salt in a reasonable time scale. From these tests the permissible utilization of the short-term load bearing capacity can be deduced, which is necessary to relate the stress dependent deformation behavior of the salt in-situ (very slow deformation rates) to lab-test conditions (relatively high deformations).

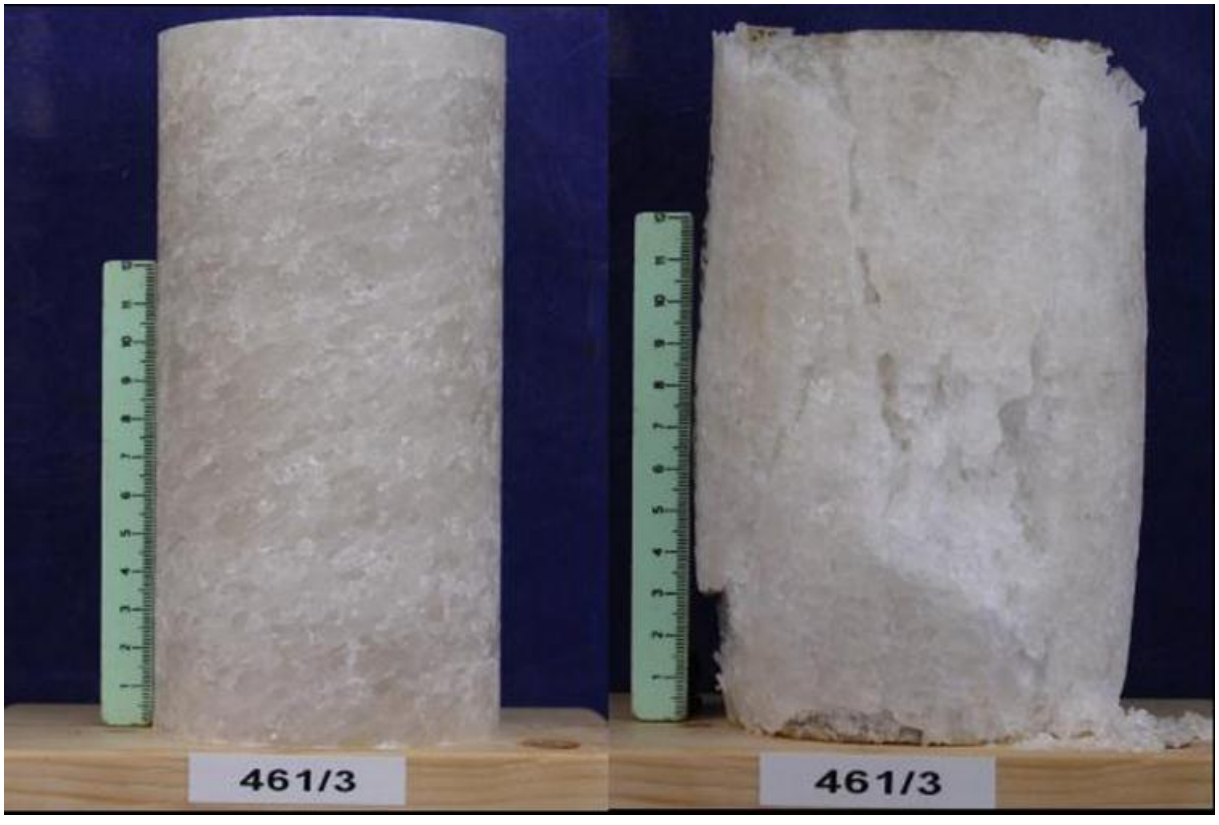

Fig: 4.1.1. Rock salt sample 461/2 before and after a triaxial compression test at low confinement

Fig: 4.1.2. Rock salt sample 461/2 before and after a triaxial compression test at high confinement

During the test the data acquisition unit is operated with a constant sampling rate collecting data from the test device such as axial deformation Δh, axial load F and the confining pressure $p = \sigma_3$. The conversion of the measured values to differential stress and strain is given by:

$$\sigma_{diff} = \left(\frac{F}{A_0} - \sigma_3 \right) \cdot (1 - \varepsilon_1) \tag{7}$$

$$\varepsilon_1 = \frac{h_0 - h}{h_0} \tag{8}$$

with:

h_0, h	length of the specimen h_0: before and h: during deformation
A_0	cross section of the undeformed specimen
F	axial load
σ_3	confining pressure

The term $(1-\varepsilon_1)$ in equation (7) results from the consideration of specimen bulging during the deformation (compression and extension), i.e. changes of the cross-section.

4.1.2. Results of triaxial compression tests

A total number of 14 specimens with a diameter of 90 mm and a height of 180 mm are tested at triaxial compression conditions including 3 specimens with relaxation phases. Selected measurement results and/or data of triaxial compression tests are presented in table 4.1.1 and table 4.1.2 and are also documented in the Annex (differential stress σ_{diff} vs. axial strain ε_1 curves).

The differential stresses σ_{diff} are always calculated as described in equation (7), i.e. these values are reduced by the change /reduction? of the cross-section resulting from lateral strain.

Table 4.1.1: Results of the strength tests - part 1 (large samples)

- Labor.-Nr.	461/06/37/TC1	461/8/52/TC2	461/11/70/TC3	461/13/85/TC4	461/18/118/TC5	461/24/165/TC6	461/27/185/TC7
σ_3 (MPa) =	0,20	20,00	0,20	0,50	10,00	0,50	1,00
σ_{Fail} (MPa) =	28,90	58,75	30,10	31,70	56,51	29,00	34,40
1_{Fail} (MPa) =	29,10	78,75	30,30	32,20	66,51	29,50	35,40
σ_{Dil} (MPa) =	11,10	29,45	9,60	11,40	24,31	8,60	11,60
ΔV_{Dil} (%) =	-0,06	-0,16	-0,04	-0,06	-0,10	-0,03	-0,03
ε_{Dil} (%) =	0,12	2,03	0,11	0,12	1,09	0,08	0,09
ΔV_{Fail} (%) =	2,38	1,60	3,59	2,55	2,40	2,97	3,69
ε_{Fail} (%) =	3,95	21,26	5,22	4,47	21,18	4,47	5,90
- Labor.-Nr.	461/30/206/TC8	461/33/226/TC9	461/39/266/TC10	461/41/280/TC11	461/43/296/TC12	461/46/317/TC13	461/50/346/TC14
σ_3 (MPa) =	1,00	2,00	2,00	4,00	4,00	7,00	7,00
σ_{Fail} (MPa) =	33,08	40,07	39,81	47,70	49,13	54,57	55,81
1_{Fail} (MPa) =	34,08	42,07	41,81	51,70	53,13	61,57	62,81
σ_{Dil} (MPa) =	11,30	12,99	16,02	19,30	21,08	23,70	24,86
ΔV_{Dil} (%) =	-0,04	-0,03	-0,06	-0,04	-0,04	-0,08	-0,08
ε_{Dil} (%) =	0,15	0,15	0,19	0,64	0,74	0,39	0,80
ΔV_{Fail} (%) =	2,62	3,82	3,18	2,84	2,26	2,17	1,80
ε_{Fail} (%) =	5,79	8,81	8,65	14,58	17,07	21,37	21,51

Table 4.1.2: Results of the strength tests - part 2 (small samples)

- Labor.-Nr.	461/8/52/K3	461/10/66/K5	461/11/70/K7	461/16/109/K9	461/16/109/K11	461/18/118/K13	461/21/144/K15	461/21/144/K16	461/21/144/K17
σ_3 (MPa) =	0,20	0,50	1,00	7,00	20,00	2,00	10,00	0,20	4,00
σ_{Fail} (MPa) =	30,30	32,70	34,30	54,60	60,40	42,90	58,60	25,20	47,50
1_{Fail} (MPa) =	30,50	33,20	35,30	61,60	80,40	44,90	68,60	25,40	51,50
ε_{Fail} (%) =	5,00	7,05	8,27	23,48	24,05	12,60	23,69	3,86	13,83
- Labor.-Nr.	461/26/178/K21	461/27/185/K23	461/27/185/K24	461/29/197/K25	461/32/217/K29	461/33/226/K31	461/33/226/K32	461/39/266/K35	461/39/266/K36
σ_3 (MPa) =	1,00	10,00	20,00	0,50	2,00	7,00	4,00	4,00	10,00
σ_{Fail} (MPa) =	32,40	58,20	61,00	27,40	40,40	55,20	46,70	47,30	57,30
1_{Fail} (MPa) =	33,40	68,20	81,00	27,90	42,40	62,20	50,70	51,30	67,30
ε_{Fail} (%) =	5,84	23,73	23,38	5,31	9,36	23,62	16,97	16,29	23,88
- Labor.-Nr.	461/41/280/K38	461/43/296/K39	461/46/317/K42	461/30/206/K44	461/33/226/K45	461/43/296/K46			
σ_3 (MPa) =	20,00	7,00	0,20	1,00	2,00	0,50			
σ_{Fail} (MPa) =	60,20	55,40	27,60	32,60	40,00	32,60			
1_{Fail} (MPa) =	80,20	62,40	27,80	33,60	42,00	33,10			
ε_{Fail} (%) =	23,73	23,94	4,08	6,93	9,46	5,80			

The average values of the static elastic parameters are determined with regard to the testing temperature of about 295 K on the basis of the test results as follows

$$E = 30 \text{ GPa}$$

$$K = 25 \text{ GPa}$$

$$\nu = 0.3$$

Static elastic parameters are generally lower than those measured dynamically. This can be attributed to the bulking effect that is induced by the coring process. Generally, it can be stated that with regard to the statistical population the same conclusion can be drawn for the elastic as for the dynamic parameters: they can be regarded to be of the same statistical population.

With regard to the stress-strain behavior the results of the triaxial strength tests on rock salt specimens at room temperature indicate that at confining pressures higher than σ_3 = 7 MPa no failure states occurred within a deformation range of up to 20 %. Obviously, the deformation behavior is characterized by a state of plastic flow.

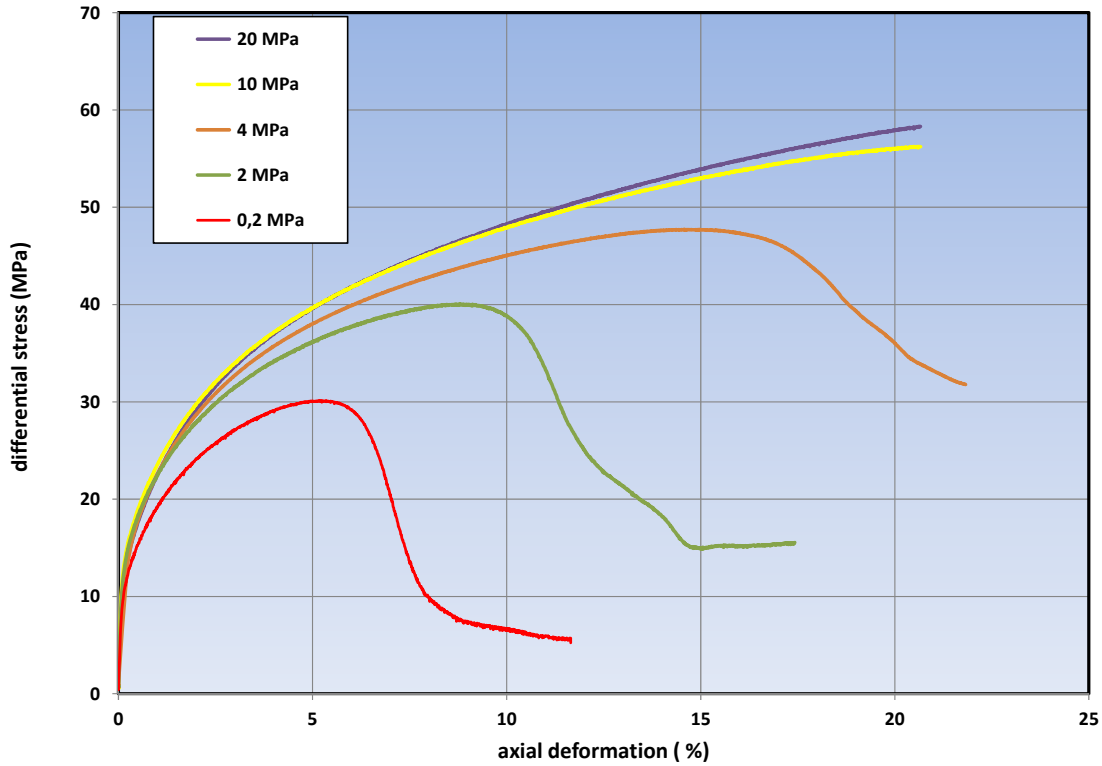

Fig: 4.1.3. Comparison of stress-strain behavior applying different confining pressures

The strength behavior of the rock salt from well ISH-01 with regard to confinement pressure can be deduced from the measured maximum values for stress difference as shown in fig 4.1.3 and 4.1.4.

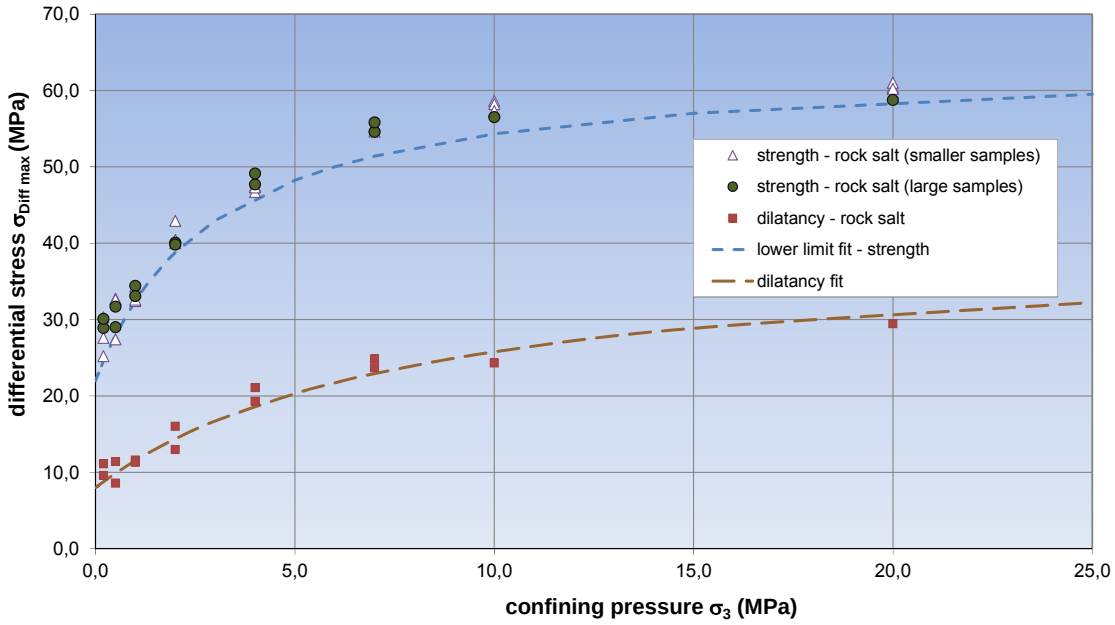

Fig. 4.1.4: Strength of all specimens from core material of ISH-01 well

In order to give a general description of this functionality, a three-parametric equation has been established resulting from an implementation of the non-linear MOHR-COULOMB failure criterion in a visco-elasto-plastic constitutive law[1] (see equation (9)).

$$\sigma_{diff,M} = \sigma_D + \left[\frac{(\sigma_{MAX} - \sigma_D)}{(\sigma_\phi + \sigma_3)} \right] \cdot \sigma_3 \qquad (9)$$

with:

σ_3	minimum principal stress,
σ_{1M}	maximum principal stress (at failure or plastic flow),
$\sigma_{diff,M} = \sigma_{1M} - \sigma_3$	maximum effective stress,
σ_D	uniaxial compressive strength,
σ_{MAX}	maximum effective strength,
σ_ϕ	curvature parameter for the strength surface.

The physical meaning of σ_{MAX} in equation (9) becomes clear, if the failure criterion is plotted as a function of $\sigma_1 - \sigma_3 = f(\sigma_3)$ (see fig. 4.1.4). Then σ_{MAX} is the maximum effective stress

[1] W. Minkley & J. Mühlbauer :"Constitutive models to describe the mechanical behaviour of salt rocks and the imbedded weakness planes"; Proc. 6th Conference on the Mechanical Behaviour of Salt, Hannover, 22-25 May 2007

which the salt can withstand (the so-called yield stress).The failure criterion moves towards with increasing minimum principal stress σ_3.

The strength behavior of ISH-01 rock salt can be given as a lower limit described by the following parameters (red line in fig. 4.1.5):

σ_ϕ = 3 MPa

σ_D = 22 MPa

σ_{MAX} = 64 MPa

As far as the maximum strength ($\sigma_{diff,M}$) is concerned, it can be stated that the values are related to the applied temperature and triaxial confinement in the range of IfG's experience.

To determine input parameters for the numerical modeling an advanced analysis of the triaxial test results is necessary.

On the basis of the visco-elasto-plastic constitutive law the material strength is determined in relation to the plastic deformation ε_p. Therefore, equation (9) needs to be expanded in a way that the dependency of the differential stress from plastic deformation $\sigma_{diff} = f(\varepsilon_p)$ can be expressed. As a prerequisite for this, the volumetric strain has to be measured during the triaxial test where two different phases of deformation can be observed. The first one is a volume compression phase until the volumetric strain has reached a minimum. Subsequently, the second phase with dilatant volume deformation starts, i.e. the volume of the specimen increases during deformation. By definition plastic deformation $\varepsilon_p = 0$ begins exactly at that point in deformation history where dilatancy is initiated. A detailed analysis of the observed stress and strain curve as well as the volumetric deformation behavior leads to the set of strength parameters in relationship to plastic deformation as shown in table 4.1.2

Table 4.1.2 Parameter for the visco-elasto-plastic constitutive law

ε_p (%)	0	0,2	0,5	1	2	4	8	12
σ_D (MPa)	8	12	14	20	25	28	2	0
σ_ϕ(MPa)	8	8	8	16	8	3	0,8	1,2
σ_{Max}(MPa)	40	42	43	40	44	45	50	58

Fig. 4.1.5 gives a representation of the strength of rock salt related to plastic deformation for ISH-01 specific rock salt material.

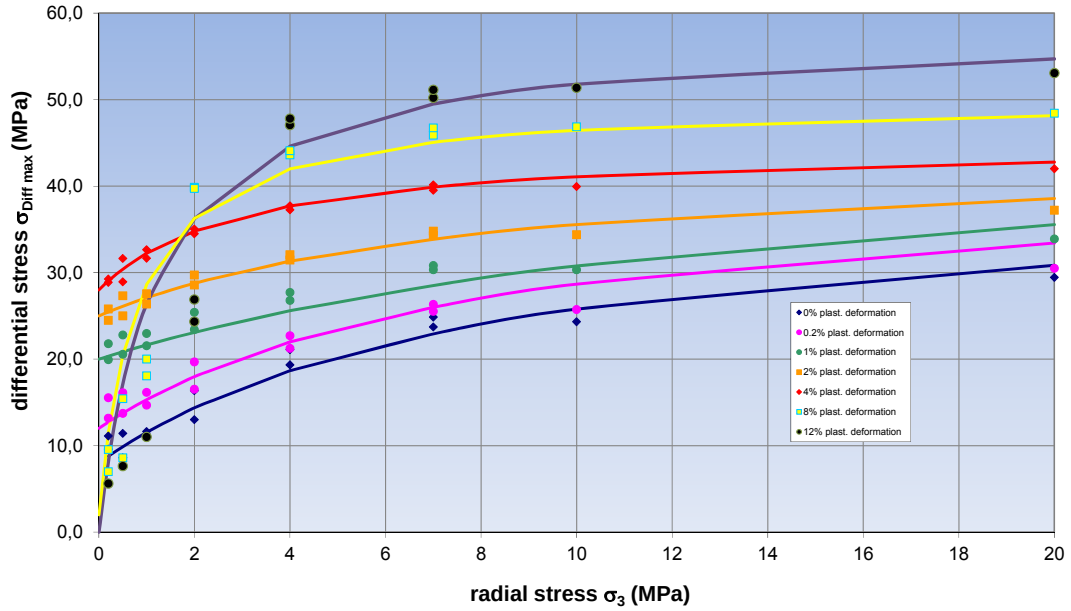

Fig. 4.1.5: Strength of ISH-01 rock salt depending on plastic deformation

The curve for 0% of plastic deformation corresponds to the dilatancy boundary. Generally known and applied constitutive laws, which include a description of the dilatancy, consider a constant dilatancy angle ψ or a constant value of the dilatancy function N_ψ. This approach is insufficient for salt rocks, because the volumetric changes ε_V of rock salt are non-linear in stress and strain as it can be seen on fig. 4.1.6 showing the volumetric strain ε_V vs. axial strain ε_1.

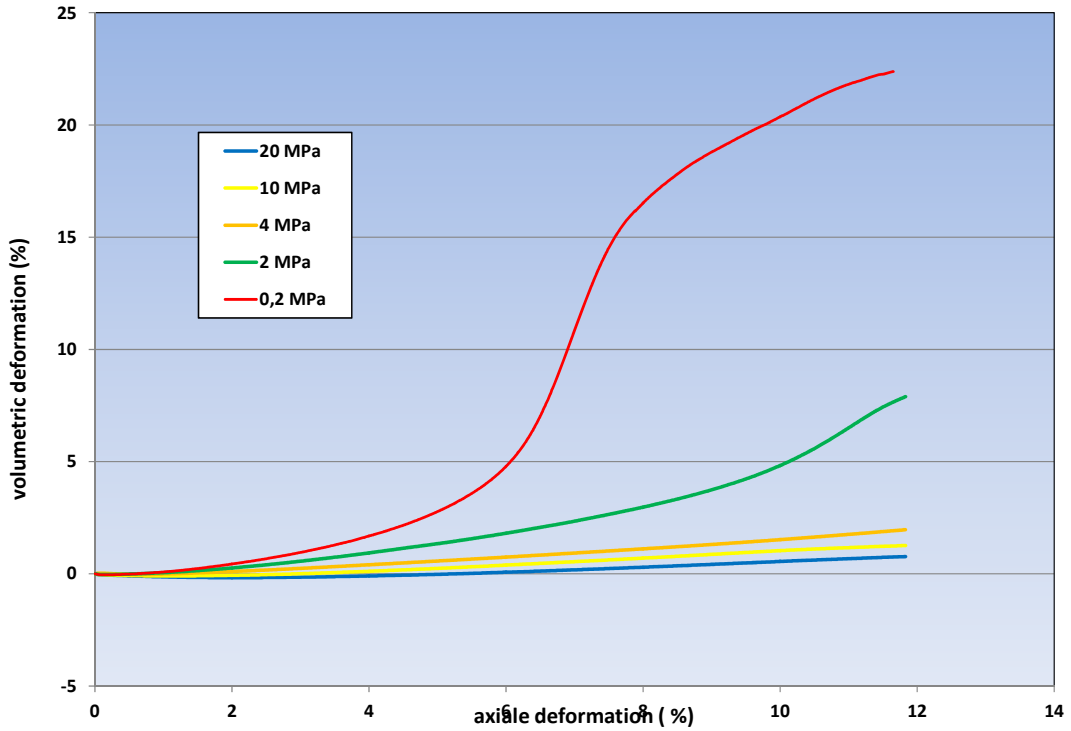

Fig. 4.1.6: Volumetric deformation during triaxial compression of ISH-01 rock salt

Obviously, the deformation induced dilatancy decreases strongly with increasing confining pressure. Therefore, the dilatancy function has to be non-linear with respect to σ_3. According to the visco-elasto-plastic constitutive law of *MINKLEY*[2], where weakening of the material is considered, equation (10) describes N_Ψ. Here, two parameters σ_Ψ and $\tan\beta_0$ are used to describe the dilatancy.

$$N_\psi = 1 + \frac{\sigma_\psi^2}{\left(\sigma_\psi + |\sigma_3|\right)^2} \cdot \tan\beta_0 \qquad (10)$$

The volume change $\Delta\left(\frac{\Delta V}{V}\right)$, which is resulting directly from the relationship between ε_V and ε_1, can be expressed by equation (11):

$$\Delta\left(\frac{\Delta V}{V_0}\right) = \varepsilon_{VOL}^P = \left(N_\psi - 1\right)\cdot \varepsilon_1^P \qquad (11)$$

Applying the functionality of volumetric strain ε_V vs. axial strain ε_1 (see fig. 4.1.6) the slope of the dilatancy curve can be determined as well as tangent or secant for each value of ε_1^p. A very simple relation results, if the slope of the secant is used as an approximation for the angle β as demonstrated by equations (12) and (13)..

$$\tan\beta = \frac{\varepsilon_{VOL}^P}{\varepsilon^P} \qquad (12)$$

$$\tan\beta = \tan\beta_0 \cdot \frac{\sigma_\psi^2}{\left(\sigma_\psi + |\sigma_3|\right)^2} \qquad (13)$$

In order to analyze the dilatancy behavior of rock salt the dilatancy boundary has to be determined, i.e. the minimum of the volumetric strain has to be identified from the observed (ε_1,ε_V)-relationship and the appropriate stress difference associated with this dilatancy boundary. The dilatancy boundary identified for tested ISH-01 rock salt material is shown in fig. 4.1.5 (line for 0% plastic strain).

By curve scanning with equidistant deformation steps additional data of $\Delta V/V_0$ (i.e. ε_{Vol}^p) were determined depending on ε_1^P. Thus, a value for tan β according to equation (13) is derived characterizing the dilatancy behavior of rock salt.

[2] MINKLEY, W., MENZEL, W., KONIETZKY, H., te KAMP, L. (2001): A visco-elasto-plastic softening model and its application for solving static and dynamic problems in potash mining. FLAC and Numerical Modeling in Geomechanics

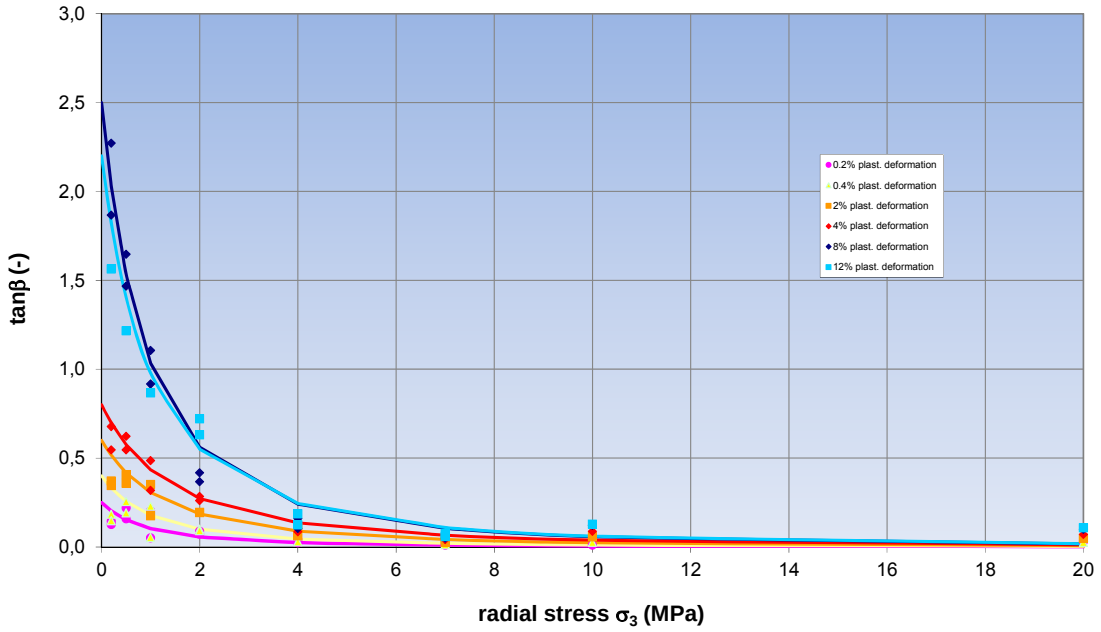

Fig. 4.1.7: tanβ-values as derived from triaxial compression tests on ISH-01 rock salt

The diagram in fig. 4.1.7 shows how the data for tanβ fit by applying equation (13). A set of curves representing different plastic deformations is visualized in order to illustrate that the test results fit quite precisely. Although the sample size is rather small a relatively good set of preliminary parameters for ISH-01 rock salt is obtained. The following table 4.1.3 summarizes the determined parameter sets describing the dilatancy by parameters σ_Ψ and tan β_0.

Table 4.1.3: Dilatancy parameter sets for rock salt from well ISH-01

plast.deformation	0,2	0,4	2	4	8	12
tanβ_0	0,25	0,4	0,6	0,8	2,5	2,2
σ_Ψ	1,8	2,0	2,5	2,8	1,8	2,0

4.2. Results of triaxial tests with relaxation phases

Special relaxation test phases during conventional triaxial tests offer a simple approach to determine the possible strength utilization. During a relaxation phase the deformation is stopped totally. If axial deformation rate is controlled at $\dot{\varepsilon}=0$ then the creep rate $\dot{\varepsilon}_{cr}$ can be calculated from equation (14), as the balance in strains $\varepsilon=\varepsilon_{cr}+\varepsilon_{el}$ results in an indirect formulation of creep strain $\dot{\varepsilon}_{el}=-\dot{\varepsilon}_{cr}$.

$$\dot{\varepsilon}_{el} = \frac{\dot{\sigma}}{E} \tag{14}$$

After loading the specimen at triaxial conditions while applying a constant deformation rate, the deformation is stopped at the level of a pre-set deformation (5% and 10 %, see Fig. 4.2.1). During the relaxation phase the differential stress decreases. Considering the observed course of the differential stress vs. time and normalizing stress data to the differential stress σ_{diff} at the beginning of the relaxation phase (t=0) a fit according to equation (15) is possible. This is needed as to obtain a value for the stress rate as stated by equation (16). In a subsequent step, the appropriate creep rate can be calculated based on equation (14) which can be related to the estimated acting differential stress.

$$\frac{\sigma_{diff}(t)}{\sigma_{diff}(0)} = \left[1 - A_0 \cdot \ln\left(1 + \frac{t}{t_0}\right)\right] \tag{15}$$

$$\dot{\sigma}_{diff} = \frac{-A_0 \cdot \sigma_{diff}(0)}{(t_0 + t)} \tag{16}$$

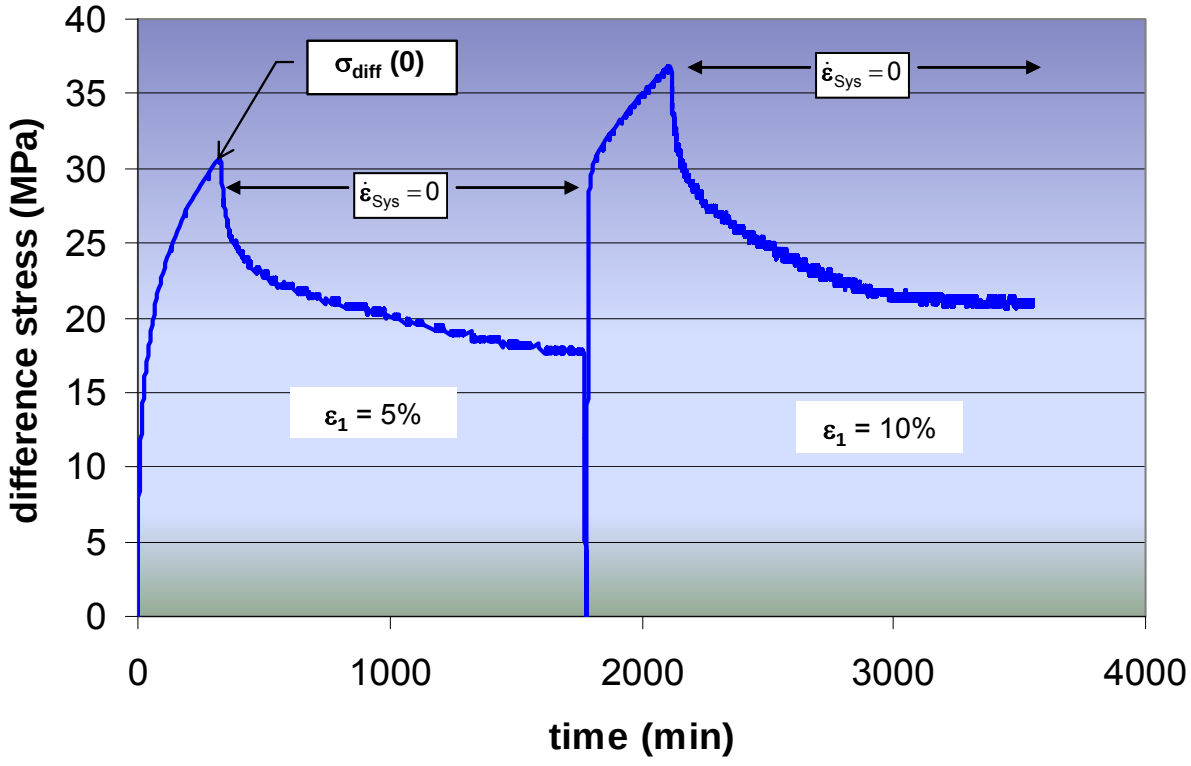

Fig. 4.2.1: Principle diagram of the relaxation test

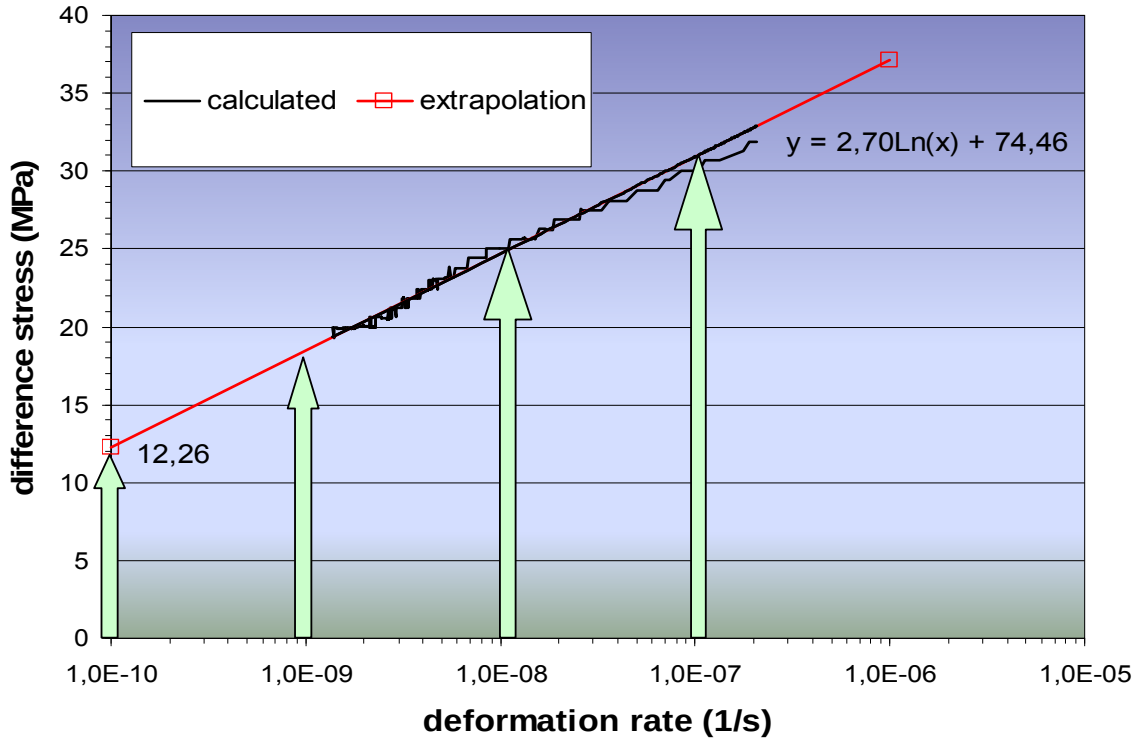

Fig. 4.2.2: Principle sketch of the relation between creep rate and stress during relaxation

The dependency of the creep rate upon the acting differential stress is presented in fig. 4.2.2, where the creep rate is scaled logarithmically. As exemplarily shown in fig. 4.2.2, a stress-strain rate relation can be obtained from the relaxation tests. Thus, it could be demonstrated that it is possible to determine long term creep behavior of the rock salt by relaxation tests.
The calculated creep rate depends logarithmically on the acting (and during the observation phase decreasing) stress. Therefore, it is possible to extrapolate two or three orders of magnitude in creep rate to find stress conditions for very low deformation rates similar to those observed in-situ.

If the above mentioned procedure is applied on the observed time dependent stress decay of ISH-01 salt material, this results in stress difference vs. strain rate as given in fig. 4.2.3. The individual stress-strain curves of the relaxations tests that have been performed with ISH-01 material as well as the interpretation of the relaxation phases are shown in the Annex.

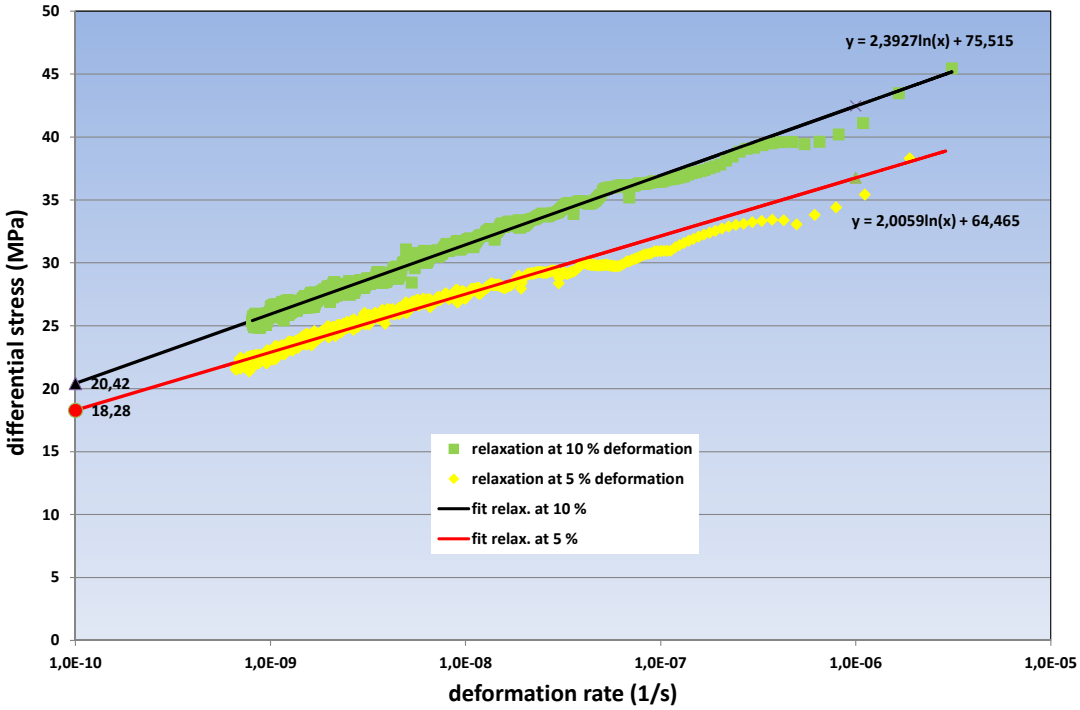

Fig. 4.2.3: Relation between creep (-strain) rate and stress from relaxation test 461/46/317/K41 at 20 MPa confining pressure

Additionally a utilization factor η can be determined in order to compare the stress dependent deformation rate observed in the laboratory with an estimated in-situ rate.

As shown in fig. 4.2.3, it is possible to extrapolate two or three orders of magnitude in creep rate to achieve stress conditions representing in-situ conditions. A utilization factor η is determined giving a relation between an assumed in-situ creep rate of $\dot{\varepsilon} = 1 \cdot 10^{-10}\,s^{-1}$ (= 0.3%/a) and the observed laboratory creep rate of $\dot{\varepsilon}_1 = 5 \cdot 10^{-6}\,s^{-1}$. This factor takes into account that the plastic flow limit of rock salt depends on the deformation rate in a manner that the plastic flow limit decreases, if the deformation rate will be reduced and vice versa.

The results of the relaxation tests are given in table 4.2.1. For the prospective cavern horizon a maximum utilization factor of 0.3 can be stated as a realistic value for a limited cavern convergence.

Table 4.2.1: Results from relaxation tests on ISH-01 rock salt

	depth (m)	confining press.	5% deform.	10% deform.	Maximum	degree of utilisation	
speciman		σ3 (MPa)	σdiff (MPa)	σdiff (MPa)	σdiff (MPa)		
			at 10^{-10}1/s	at 10^{-10}1/s		5% deform.	10% deform.
461/46/317/K41	925	20	18,28	20,42	57,6	0,32	0,35
461/29/197/K27	822	20	19,63	##	58,4	0,34	##
461/23/158/K19	789	20	20,45	23,29	59,96	0,34	0,39

If the well known rheological model of a BURGER'S-model (see fig. 6.2.3) is assumed as material model for the creep behavior of rock salt, the viscosity of its MAXWELL-part represents the secondary creep rate, which can be calculated by dividing the observed stresses by the appropriately related creep rates. These values for the MAXWELL-viscosity η_M are exponentially depending on the level of the stress difference (see fig. 4.2.4).

$$IfG - Approach\ (according\ to\ fig.4.2.4)$$

$Creep\,(all\ tests)$	$\mathrm{Re}\,laxation$
$\eta_0 = 1.86 \cdot 10^6\ \ MPa \cdot d$	$\eta_0 = 1.08 \cdot 10^{10}\ \ MPa \cdot d$
$m = 0.164$	$m = 0.421$

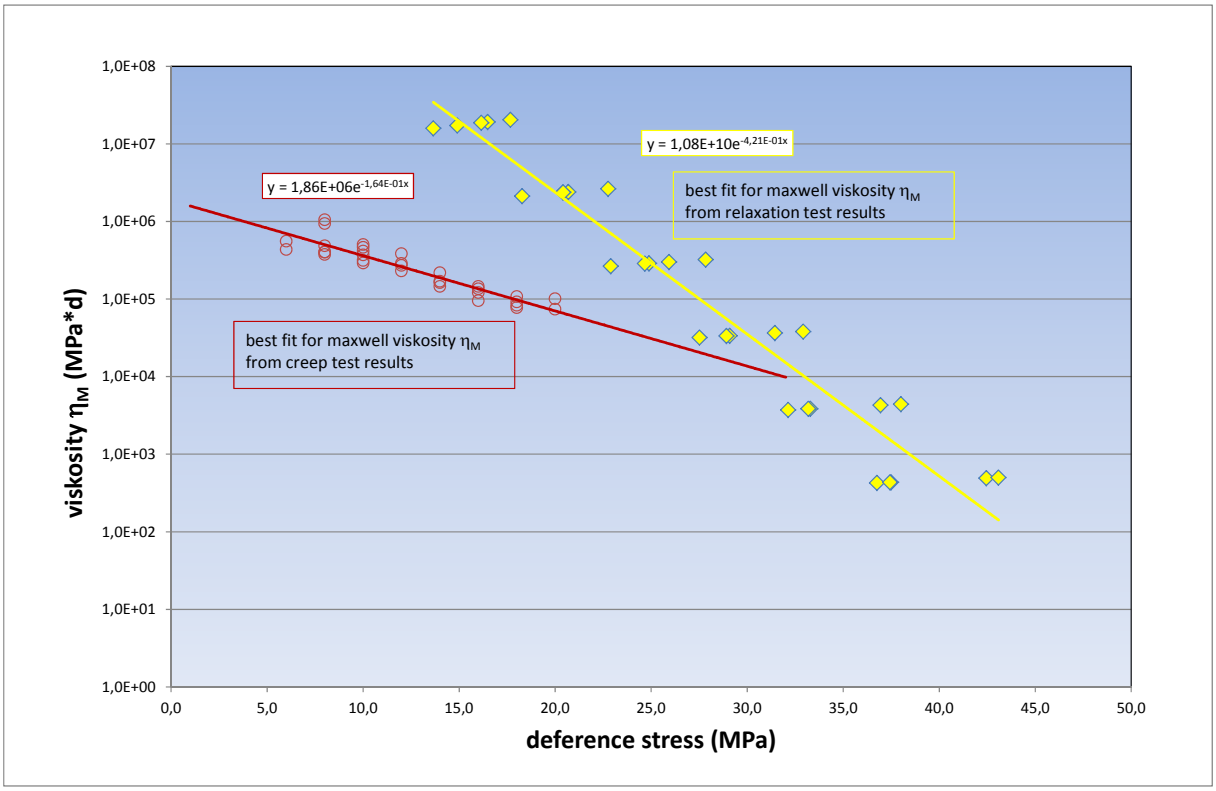

Fig. 4.2.4: η_M - viscosities from relaxation test compared to those derived from creep tests

5. Shear tests on anhydrite interfaces of the rock salt

For a description of a failure criterion the knowledge of the strength parameters of the material is absolutely essential. In any case when bedding planes exist in foliated rocks which are probably the clearest example of existing interfaces (e.g. MINKLEY & MÜHLBAUER, 2007)[7], additionally to rock joints and other geomechanical discontinuities ,.then the mechanical properties of these interfaces have to be determined.

For the mechanical behavior of interfaces the relevant variables

- stress traction vector with one normal component and one tangential in a simple 2-dimensional stress field (or two tangential in a 3-dimensional stress field), and
- the conjugate "strain" variables

are the corresponding relative displacements. However, such stress conditions can be only realized in direct shear tests, which are therefore of urgent need to reproduce slip between various materials.

5.1. Test procedure

The slip criterion for geomaterials (or for a plane of weakness in the strata, e.g. bedding planes) is referred in the literature to many different terms: shear strength, failure criterion, yield criterion, or Coulomb criterion. It is expressed often as an equation that stipulates the maximum permissible shear stress along the slip surface being analyzed. The simplest linear form, the linear MOHR-COULOMB (MC) criterion, may be written as

$$\tau_{max} = c' + \sigma'_n \cdot \tan \Phi' \qquad (17)$$

with

τ_{max}	maximum shear stress that the plane can sustain before slipping,
c'	cohesion of the rock,
σ'_n	normal effective stress across the slipping plane, and
Φ'	angle of internal friction.

The material parameters c' and Φ' are determined empirically from testing results.

In the past, several companies have developed improved state-of-the-art testing equipment, which allows new types of testing procedures in order to determine the mechanical parameters of joints and intact rock. High-response servo-hydraulic systems with digital control technology, strain measurement equipment mounted onto the specimen and programmable control modes enable new types of test procedures, which are tailored to the specific problem, e.g. BLUEMEL (2000)[3]; BLUEMEL & POETSCH (2003)[4]. For the realization of shear tests required for the samples of well ISH-01 a modern shear test system is available at the IfG (fig. 2.2).

[3] BLUEMEL, M., 2000. Improved procedures for laboratory rock testing. EUROCK 2000. ISRM Symposium Aachen, 573 – 578.

[4] BLUEMEL, M., POETSCH, M., 2003. Direct shear testing system. International Symposium on GeoTechnical Measurements and Modelling, Karlsruhe, 327 – 331.

The loading frame consists of a two-axle experimental setup with vertical and horizontal stress initiation, a platform for shear testing in a shear box, and a servo-hydraulic control unit for two channels (vertical and horizontal deformation). Both can be controlled in terms of applied forces or displacements. The test arrangement is shown in fig. 5.1.1. The front part (on the right side) is realized by an extremely stiff four-columned test frame for fixing and vertical loading of the two-part shear box by the upper hydraulic cylinder (up to 500 kN axial load).

While a vertical load acts on the whole shear box the lower box can be horizontally displaced under the applied loads. The layout of the deformation measurement system by Linear Variable Differential Transformers (LVDT), which can be positioned at the initial specimen joint shear plane in multiple locations (4 vertical and 2 horizontal LVDT), guarantees that the dilatancy, the shear displacement and the rotations can accurately be measured.

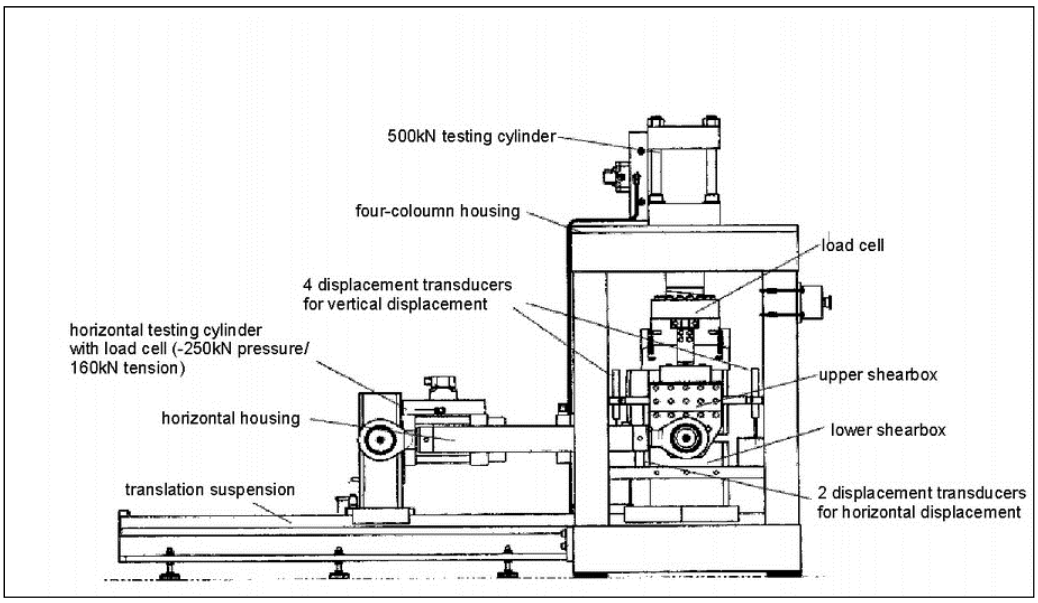

Fig. 5.1.1: Schematic sketch of the MTS – test system with the direct shear assembly.

A sufficiently stiff fixing of the specimens is a prerequisite for an exact determination of shear resistance. Therefore, first of all the specimen is orientated in a position where the line of action of the shear force (τ_T) is adjusted to the investigated interface and the line of action of the normal stress (σ_n) is perpendicularly to that plane. Subsequently, both shear boxes are filled in succession with high-strength anchor cement mortar. An approx. 20 mm opening remains that enables the shear testing of the fixed specimen (see fig. 5.1.2).

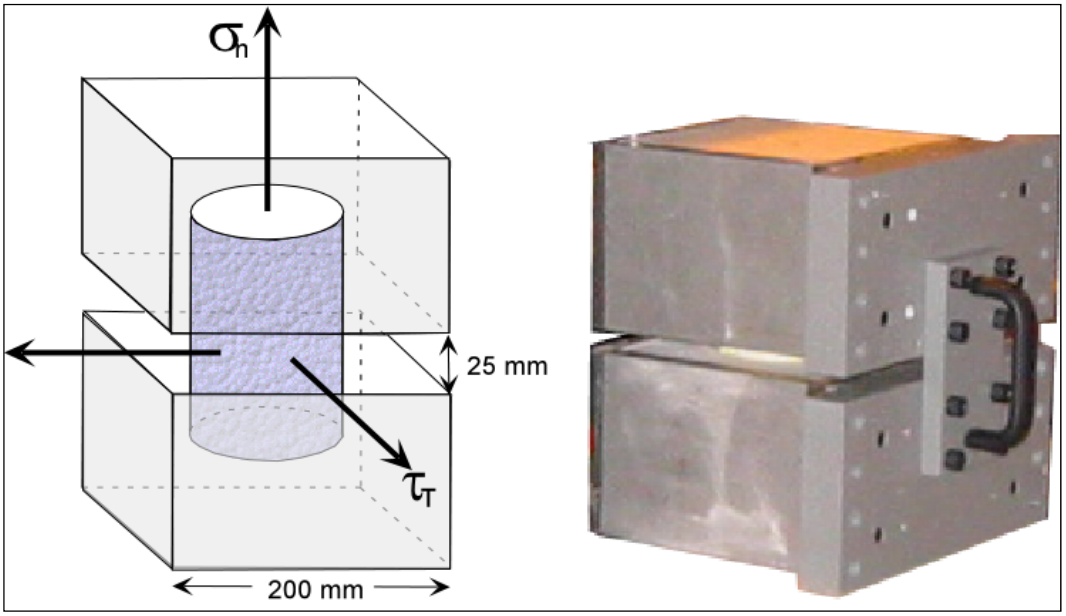

Fig. 5.1.2: Two-parts shear box for shear tests: (Left) Schematic sketch with orientation of the specimen and the 20 mm opening between the two single boxes. (Right) prepared box with installed cylindrical specimen.

5.2. Results of direct shear tests (SV)

Two types of direct shear tests are generally performed at the IfG Leipzig laboratories for determining shear strength parameters:

1. direct shear tests under constant normal load conditions, and
2. direct shear tests under dilatancy-free conditions (without vertical deformation).

Only type 1 was performed on ISH-01 specimens as follows: for characterization of the mechanical behavior of the bedding plane a constant normal stress is applied at a certain level and then kept constant while shear related displacements is applied to the specimen. The measured values include shear stress and normal relative displacement, in addition to dilatancy, e.g., compaction or up-gliding corresponding to displacement in the direction of σ_n. The test is continued in two steps with increased values of normal stress focusing on the residual strength. Therefore, the shear stress increases with further shear deformation until the sample fails at the weakening plane (maximum peak value). Then, the shear strength reduces up to a plateau: the residual strength.

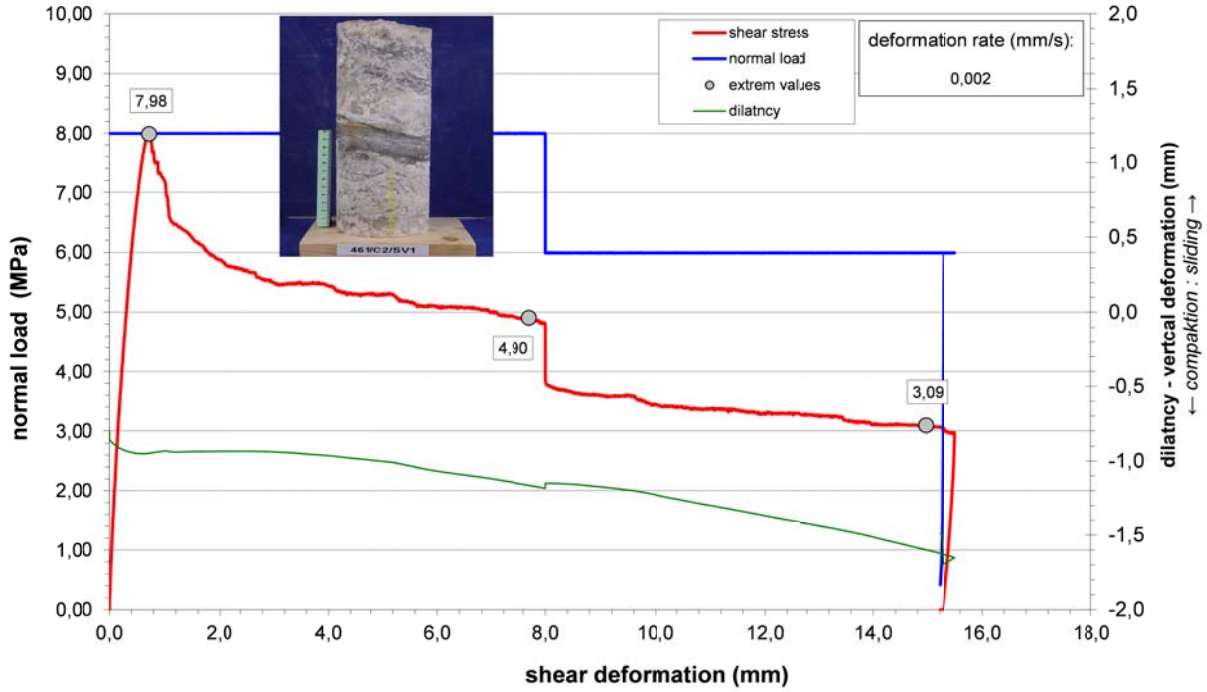

Fig. 5.2.1: Direct shear test overview – test results of specimen 461-C2-SV1.

in a combined shear strength and dilatancy diagram (see fig. 5.2.1), each test delivers the following results:

- Shear strength curve: Shear stress usually grows in an elastic manner up to a peak and then drops down to a residual value. Peak and residual values become higher with applied normal stress.
- Dilatancy curve: Due to the surface roughness and asperities, joints tend to dilate upon shear; this effect tends to level off after a certain amount of prescribed shear displacement, and is lower for higher normal stress because a slide over of joint surfaces is suppressed.

#

5.3. Results of direct shear tests (SV)

Five direct shear test with normal loads between σ_n = 4 and 16 MPa were performed on rock salt of the well ISH-01. The gained strength values at accordant normal load conditions are given below (Tab. 3.5-2).

Tab. 5.3.1: Shear test loading conditions and determined strength values.

		σ_n	τ
test	**step**	**(MPa)**	**(MPa)**
SV1	$\sigma_{step\ 1}$ = 8,00 MPa	8,00	7,98
	$\sigma_{step\ 1}$ = 8,00 MPa	8,00	4,90
	$\sigma_{step\ 2}$ = 6,00 MPa	6,00	3,09
SV2	$\sigma_{step\ 1}$ = 10,00 MPa	10,00	8,99
	$\sigma_{step\ 1}$ = 10,00 MPa	10,00	6,01
	$\sigma_{step\ 2}$ = 11,00 MPa	11,00	5,46
SV3	$\sigma_{step\ 1}$ = 12,00 MPa	12,00	9,61
	$\sigma_{step\ 1}$ = 12,00 MPa	12,00	4,93
	$\sigma_{step\ 2}$ = 13,00 MPa	13,00	4,31
SV4	$\sigma_{step\ 1}$ = 14,00 MPa	14,00	9,20
	$\sigma_{step\ 1}$ = 14,00 MPa	14,00	7,25
	$\sigma_{step\ 2}$ = 16,00 MPa	16,00	7,62
SV5	$\sigma_{step\ 1}$ = 4,00 MPa	4,00	6,61
	$\sigma_{step\ 1}$ = 4,00 MPa	4,00	2,98
	$\sigma_{step\ 2}$ = 6,00 MPa	6,00	4,04

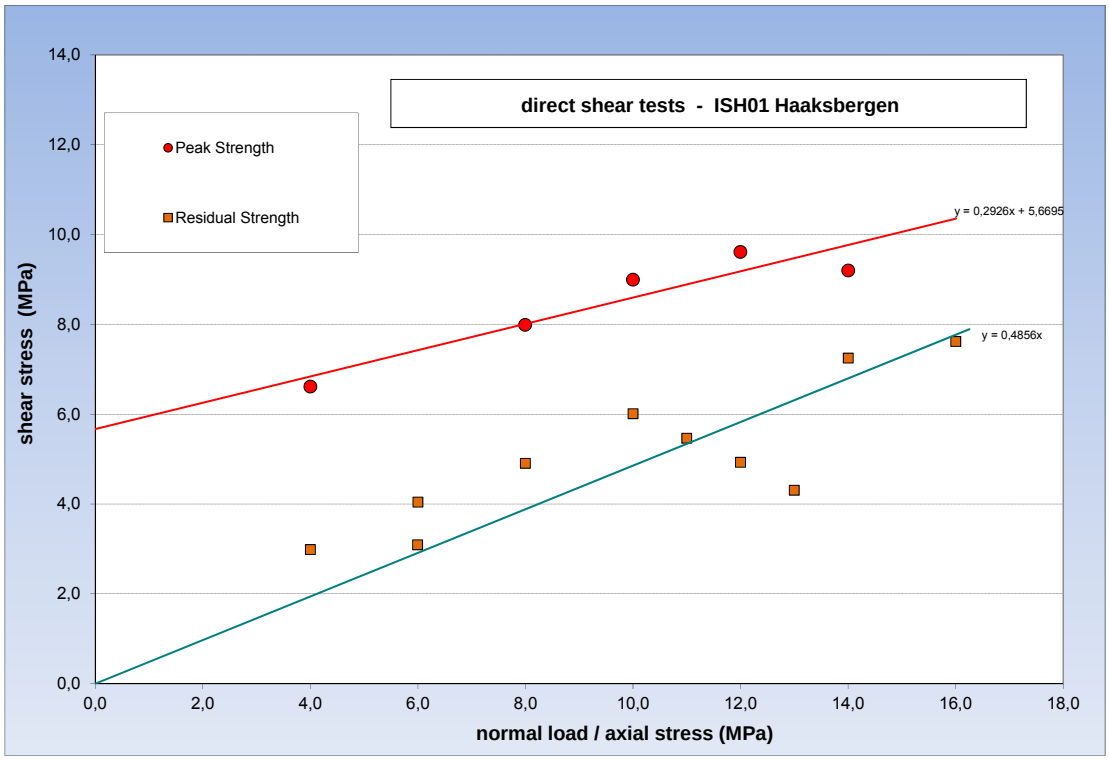

Fig. 5.3.1: Direct shear tests on rock salt of well ISH-01.

According to fig. 5.3.1 the following MOHR-COULOMB-parameters were derived as:

$\tau = c + \sigma_N \cdot \tan\varphi$	C	φ
	(MPa)	(°)
	5,67	16,3
residual shear strength	0,00	25,9

6. Creep tests

6.1. Creep test procedure

The creep tests were carried out at temperatures of 318 K applying triaxial load conditions during a test period of 60 to 80 days. The testing temperature for the creep test has been adapted to in-situ conditions at the extraction depth of the cores. The manufactured diameter of the specimen is d = 40 mm and their height h = 80 mm. These values are limited by the test device. In total 6 creep tests were performed at different triaxial test conditions as documented in table 4.2.1.

The axial stress results from a mechanical load device similar to a pair of balance, which can be used up to 200 kN. The confining pressure results from a hydraulic system and is kept constant by an accumulator (see fig. 2.3). Deformation measurement is carried out using three gages fixed around the samples, each with an offset of 120°. The accuracy of the measured deformation is less equal to $\pm$ 0.001 mm.

The axial load is applied stepwise by means of a calibrated load cell. The confining pressure is measured by pressure transducers. Both, load and pressure are kept constant with an accuracy of ± 1% during the tests. After loading to hydrostatic conditions and keeping for 24 hours at constant temperature the samples are loaded by increasing the axial stress with a rate $\dot{\sigma}_1$ = 1 MPa/min. The first deformation measurement immediately after the loading phase leads to the starting values for creep deformation $\Delta h_{cr}(0)$ at the lifetime t=0 of the experiment. If necessary, the axial load is stepwise increased during the test period in order to compensate the increase of the cross-section generated by the lateral strain according to equation (18) and thus maintaining a constant stress. Thereby the appropriate cross-section is assumed as a function of axial strain.

$$A(\varepsilon) = \frac{A_0}{(1-\varepsilon)} \tag{18}$$

with

$$\varepsilon = \frac{\Delta h}{h_0} \tag{18a}$$

All test parameters such as deformation, confining pressure and temperature are checked and recorded daily.

6.2. Creep test results

The results of the performed creep tests are shown individually in Annex 51 to Annex 66 as diagrams of the creep deformation vs. testing time. Secondary (steady state) creep rates are determined using a linear fit for measured creep deformation data during the last period of the tests. The resulting creep rates are listed in table 6.2.1.

Table 6.2.1: Results from ISH - 01 creep tests – secondary creep rate

specimen	load step	load (MPa)			rate (1/d)
		σ_1	σ_3	$\Delta\sigma$	
461/8/52/K2	1	38	20	18	2,32E-04
	2	40	20	20	2,71E-04
461/8/52/K4	1	38	20	18	1,67E-04
	2	40	20	20	1,98E-04
461/10/66/K6	1	36	20	16	1,18E-04
	2	38	20	18	1,96E-04
461/11/70/K8	1	36	20	16	1,68E-04
	2	38	20	18	2,16E-04
461/16/109/K10	1	34	20	14	9,63E-05
	2	36	20	16	1,32E-04
461/16/109/K12	1	34	20	14	8,62E-05
	2	36	20	16	1,10E-04
461/18/118/K14	1	32	20	12	5,20E-05
	2	34	20	14	8,26E-05
461/21/144/K18	1	32	20	12	4,16E-05
	2	34	20	14	6,42E-05
461/23/158/K20	1	30	20	10	3,44E-05
	2	32	20	12	4,43E-05
461/26/178/K22	1	30	20	10	3,18E-05
	2	32	20	12	3,13E-05
461/29/197/K26	1	28	20	8	1,65E-05
	2	30	20	10	1,98E-05
461/29/197/K28	1	28	20	8	1,99E-05
	2	30	20	10	2,41E-05
461/32/217/K30	1	28	20	8	1,99E-05
	2	30	20	10	2,69E-05
461/38/262/K34	1	28	20	8	2,13E-05
	2	30	20	10	2,15E-05
461/41/280/K37	1	26	20	6	1,08E-05
	2	28	20	8	7,62E-06
461/43/296/K40	1	26	20	6	1,38E-05
	2	28	20	8	8,50E-06

A total of 16 specimens was tested at two load stages. The applied deviatoric stresses are in a range of 6 and 20 MPa, while a confining pressure between 5 to 15 MPa was applied.

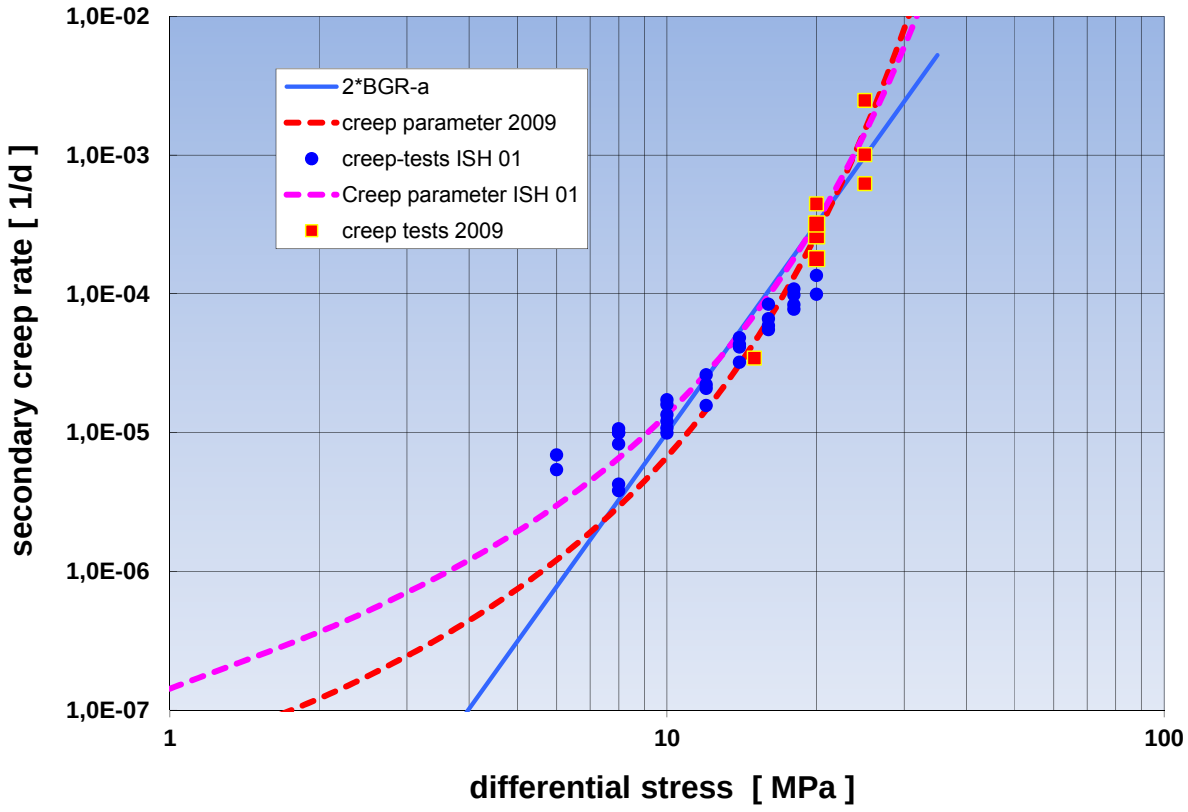

Fig. 6. 2.1: Results of the long-term creep tests on rock salt from ISH-01 compared to results from other locations and with BGR approach

Fitted secondary creep rates as given in fig. 6.2.1 can be used to determine the parameters for the NORTON creep law as described by equation (19).

$$\dot{\varepsilon}_{creep} = \dot{\varepsilon}_0 \cdot \sigma_{diff}^{n} \qquad (19)$$

This material law is a power law approach with two parameters: the intrinsic creep rate $\dot{\varepsilon}_0$ and the stress exponent n.

The NORTON power law is used to compare the test results in a very simple manner with data of former investigations on salts from other locations investigated by the BGR (two times BGR-a is used).

Further test analysis was made in order to identify parameters for the generalized non-linear MOHR-COULOMB plasticity model after MINKLEY[5], where the creep behavior is described by a

[5] W. Minkley & J. Mühlbauer :"Constitutive models to describe the mechanical behaviour of salt rocks and the imbedded weakness planes"; Proc. 6th Conference on the Mechanical Behaviour of Salt, Hannover, 22-25 May 2007

modified BURGER'S model. Besides the skleronom material properties (not depending on time) most saline rocks are characterized by rheonom or viscose properties (depending on time), i.e. they are showing a time-dependent stress-strain behavior. The visco-elasto-plastic constitutive law according to MINKLEY, separates the deformation as follows:

ε^K: retarded elastic deformation
(KELVIN- model: a spring with a parallel viscose damper)

ε^M: visco-elastic deformation
(MAXWELL - Model: a spring in line with a viscose damper)

ε^P: plastic deformation
(modified non-linear MOHR-COULOMB - model with softening and dilatancy).

Summing up these three individual contributions yields the total deformation.. Combining the BURGERS creep model with the generalized non-linear MOHR-COULOMB model which includes softening and dilatancy (compare fig.6.2.3), a model is established describing the creep behavior of rock salt in greater detail. This model presents a more realistic material behavior of salts incorporating primary and secondary creep and at the same time including the accelerated tertiary creep phase, which is caused by dilatant softening processes. The primary creep phase is modeled by the Kelvin mechanism characterized by the KELVIN shear modulus G^K and the KELVIN viscosity η^K. Both, the shear modulus G^K and the viscosity η^K are assumed to be depending exponentially on the deviatoric stress σ_V (equal to σ_{diff}).

$$\eta^K = \eta_0^K \cdot e^{-n_1 \cdot \sigma_V} \qquad (19)$$

$$G^K = G_0^K \cdot e^{-n_2 \cdot \sigma_V} \qquad (20)$$

The secondary creep phase is controlled by the Maxwell viscosity η^M. The tertiary creep phase which ends up with creep rupture is governed by a dilation softening mechanism.

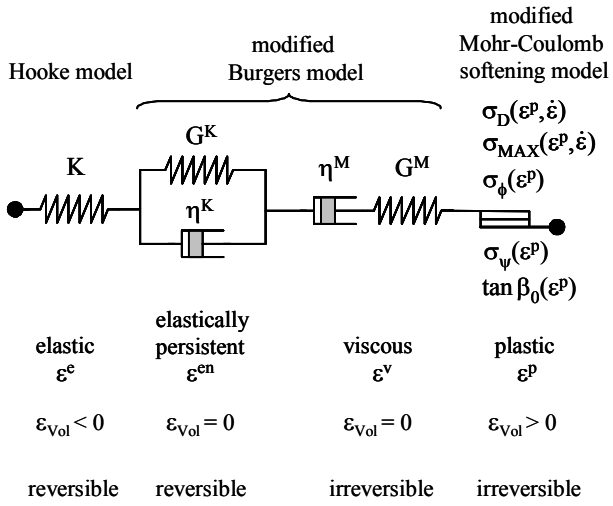

Fig. 6.2.3: Visco-elasto-plastic model with the modified Burger's body

Within the visco-elasto-plastic material model of MINKLEY, the stress dependency of the creep rate is defined by an exponential dependency of the Maxwell viscosity η^M on the deviatoric stress σ_V, which is defined in the modified BURGHERS mechanism:

$$\eta^M = \eta_0^M \cdot e^{-m \cdot \sigma_V} \qquad (21)$$

In order to demonstrate the quality of MINKLEY model the back-calculation of a creep test is shown exemplarily in fig. 6.2.4 in terms of creep deformation vs. time. On this diagram the good accordance of measured and back-calculated values is visible.

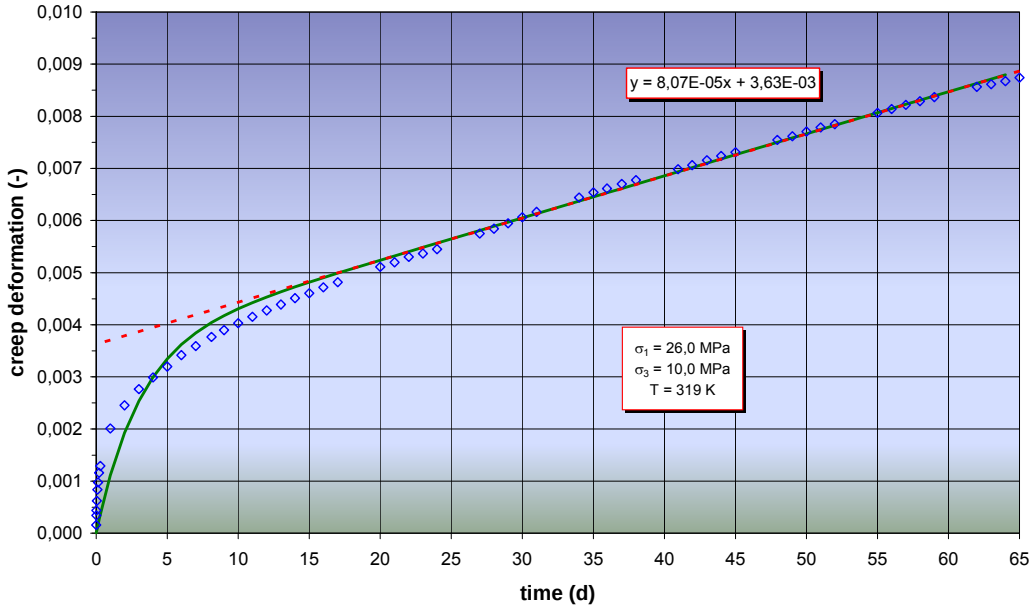

Fig. 6.2.4: *Creep behaviour of a rock salt specimen fitted by the BURGERS-model*

In order to extract material parameters from the results of the creep tests, which then can be used as input for the above described material law of MINKLEY, measurement results of the well ISH-01 creep tests are plotted next to each other (see fig. 6.2.5).

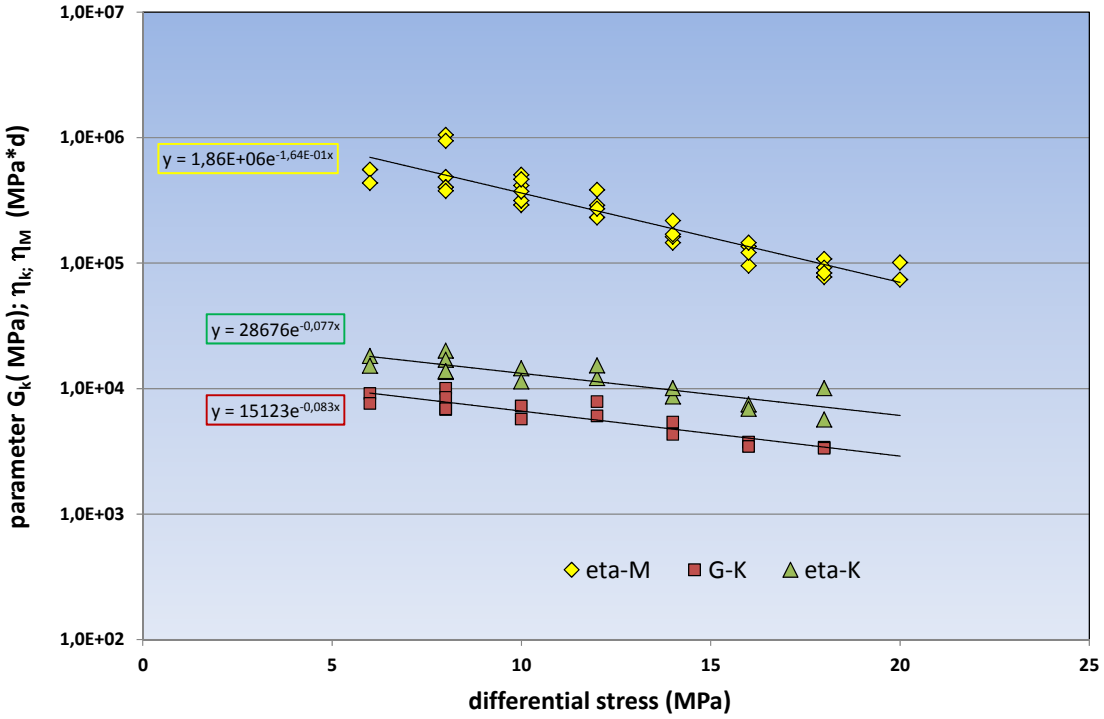

Fig. 6.2.5: Parameter determination - BURGERS-model

Table 6.2.2 represents a summary of the fitted parameters.

The performed investigation program provides a reliable data basis for the description of the creep properties of site-specific rock salt with regard to the well ISH-01. Variations of the determined characteristic parameters still remain within a small scatter when considering experiences in testing of various rock salts.

Table 6.2.2: Creep parameters for the visco – elasto - plastic model

Parameter	$\eta_0^M \; G_0^K \; \eta_0^K$	m, n_2, n_1
η_M (MPa*d)	$1.86 * 10^6$	0,164
G_K (MPa)	$1,51 * 10^4$	0,077
η_K (MPa*d)	$2,87 * 10^4$	0,083

Table 6.2.3: Results of the creep tests – analyses of the Burgers-parameter

specimen	load step	load (MPa)			ηM	Gk	ηk (MPa*d)
		σ_1	σ_3	Δσ	(MPa*d)	(MPa)	(MPa*d)
461/8/52/K2	1	38	20	18	7,76E+04	3,40E+03	5,67E+03
	2	40	20	20	7,38E+04		
461/8/52/K4	1	38	20	18	1,08E+05	3,34E+03	1,01E+04
	2	40	20	20	1,01E+05		
461/10/66/K6	1	36	20	16	1,36E+05	3,74E+03	7,47E+03
	2	38	20	18	9,18E+04		
461/11/70/K8	1	36	20	16	9,52E+04	3,45E+03	6,90E+03
	2	38	20	18	8,33E+04		
461/16/109/K10	1	34	20	14	1,45E+05	4,32E+03	8,65E+03
	2	36	20	16	1,21E+05		
461/16/109/K12	1	34	20	14	1,62E+05	5,40E+03	1,01E+04
	2	36	20	16	1,45E+05		
461/18/118/K14	1	32	20	12	2,31E+05	6,06E+03	1,21E+04
	2	34	20	14	1,69E+05		
461/21/144/K18	1	32	20	12	2,88E+05	7,86E+03	1,53E+04
	2	34	20	14	2,18E+05		
461/23/158/K20	1	30	20	10	2,91E+05	7,25E+03	1,45E+04
	2	32	20	12	2,71E+05		
461/26/178/K22	1	30	20	10	3,14E+05	5,70E+03	1,14E+04
	2	32	20	12	3,83E+05		
461/29/197/K26	1	28	20	8	4,85E+05	1,00E+04	2,01E+04
	2	30	20	10	5,05E+05		
461/29/197/K28	1	28	20	8	4,02E+05	8,50E+03	1,70E+04
	2	30	20	10	4,15E+05		
461/32/217/K30	1	28	20	8	4,02E+05	6,80E+03	1,36E+04
	2	30	20	10	3,72E+05		
461/38/262/K34	1	28	20	8	3,76E+05	6,90E+03	1,38E+04
	2	30	20	10	4,65E+05		
461/41/280/K37	1	26	20	6	5,56E+05	9,14E+03	1,82E+04
	2	28	20	8	1,05E+06		
461/43/296/K40	1	26	20	6	4,35E+05	7,60E+03	1,52E+04
	2	28	20	8	9,41E+05		

7. Summary

In the context of developing a cavern construction project in new areas in the eastern Netherlands and from deeper layers of the Permian Zechstein salt the Institute for Geomechanics – Leipzig was asked by DEEP. Underground Engineering GmbH, Bad Zwischenahn to realize rock-mechanical investigations.

This report presents the results of the rock-mechanical laboratory investigations on core material from the well ISH-01. The tests are carried out in 2012. In total 64 specimens, representing the designed setting depth of the planned caverns in the Haaksbergen area, are investigated at room temperatures.

The test program comprises short-term strength and deformation tests on rock salt samples as well as long-term creep and relaxation tests in order to investigate the creep behavior. The concept of the rock-mechanical test program aims at a

- lithological characterization/determination of petrophysical parameters– e.g. density, ultrasonic properties
- investigation of short-term strength and dilatancy properties, i.e. realization of triaxial short-term tests at various confining pressures
- investigation of possible weakness planes (i.e. bedding planes or lithological rock interfaces) with direct shear tests
- investigation of the long-term properties, i.e. realization of triaxial compression relaxation and creep tests.

Furthermore, the tests are carried out in order to determine input parameters for the material law that subsequently will be used in the numerical modeling of a generic cavern. This generic cavern will be the representative cavern according to the production planning for Haaksbergen. These numerical simulations will investigate the possible future operations of the planned brine production caverns.

Short-term triaxial compression tests with simultaneous measurements of the volumetric strain (dilatancy) are performed at confining pressures between 0.2 and 20 MPa in order to determine the strength parameter set for the subsequent modeling. By means of the results of the triaxial strength tests it can be stated that no failure will occur as far as the confinement of the specimens remains in the range of the expected typical depth dependent minimum principle stress, which can be related to the brine column pressure.

Because bedding planes in foliated rocks in addition to rock joints and other geo-mechanical discontinuities may act as weakness planes in the rock mass, direct shear tests are performed on core samples representing interfaces between salt and anhydrite. For a description of material failure criterion the knowledge of its strength parameters is needed. Using the direct shear test system, available at IfG's, shear strength properties, i.e. MOHR-COULOMB parameters are determined for interfaces inside the salt portions.

Furthermore, in order to provide input parameters for the modeling of the creep behavior, characteristic values for the visco-elasto-plastic model parameters for the modified BURGER'S model were determined. These parameters, which are given in table 6.2.2, differ from those known for Zechstein 2 salt. Generally, it can be stated that the investigated rock salt from the Zechstein (Werra)1 Formation tends to have a higher creep behavior. Taking into account all conditions (especially the observation time) the creep deformation is slightly higher than expected.

The utilization factors, describing the relationship between the acting stress difference within a rock element surrounding the cavern and the maximum stress difference determined in the laboratory are typically in the range of 0.2 and 0.4. This range is confirmed by the results of the relaxation tests.

Analyzing the results of the laboratory tests (carried out in line with this order), it can be stated that the strength and deformation parameter sets are valid for active loading conditions (leaching) and time dependent inner deformation as well as stress relocation processes (creep and relaxation) at well ISH-01. Therefore, the determined parameters for the selected constitutive law for rock salt can be used to simulate the leaching operation of a prospective generic cavern representing the planned Haaksbergen brine production site. The necessary numerical modelling will be done in a subsequent step in order to prove the long-term stability and tightness and to describe the convergence behavior of the caverns.

List of Appendices